Structural Engineering and Mechanics, *Vol. 69, No. 6 (2019) 677-691*
DOI: https://doi.org/10.12989/sem.2019.69.6.677

Experimental vs. theoretical out-of-plane seismic response of URM infill walls in RC frames

Gerardo M. Verderame[a], Paolo Ricci[b] and Mariano Di Domenico*

Department of Structures for Engineering and Architecture, University of Naples Federico II Via Claudio 21 – 80125 – Naples, Italy

(Received May 3, 2018, Revised January 26, 2019, Accepted February 5, 2019)

Abstract. In recent years, interest is growing in the engineering community on the experimental assessment and the theoretical prediction of the out-of-plane (OOP) seismic response of unreinforced masonry (URM) infills, which are widespread in Reinforced Concrete (RC) buildings in Europe and in the Mediterranean area. In the literature, some mechanical-based models for the prediction of the entire OOP force-displacement response have been formulated and proposed. However, the small number of experimental tests currently available has not allowed, up to current times, a robust and reliable evaluation of the predictive capacity of such response models. To enrich the currently available experimental database, six pure OOP tests on URM infills in RC frames were carried out at the Department of Structures for Engineering and Architecture of the University of Naples Federico II. Test specimens were built with the same materials and were different only for the thickness of the infill walls and for the number of their edges mortared to the confining elements of the RC frames. In this paper, the results of these experimental tests are briefly recalled. The main aim of this study is comparing the experimental response of test specimens with the prediction of mechanical models presented in the literature, in order to assess their effectiveness and contribute to the definition of a robust and reliable model for the evaluation of the OOP seismic response of URM infill walls.

Keywords: URM infill wall; experimental; mechanical; out-of-plane strength; out-of-plane response; arching action; stripe method

1. Introduction

An unreinforced masonry (URM) infill wall can withstand out-of-plane (OOP) seismic loads by the development, after cracking, of internal arching thrusts. In fact, the inclined arching thrusts forming in the infill panel thickness have a resultant horizontal component that equilibrates the OOP external load. This resistant mechanism is called “arching action”. Arching thrusts can form only if the infill wall is adequately thick and supported by sufficiently stiff and resistant confining structural elements (ASCE/SEI 41-13 2013). Usually, infill walls are mortared and, so, restrained along four edges to the confining structural elements. This enables two-way (both horizontal and vertical) arching action occurring. In infill walls bounded only along the upper and the lower edge to the confining structural elements, as well as in URM walls, only one-way vertical arching can occur. In infills bounded to the confining elements along the lower and both the lateral edges, only one-way horizontal arching can occur.

In the literature, different studies concerning the experimental assessment and modelling of the OOP behaviour of URM infills and walls in which arching action occurs have been proposed in recent years (e.g., Agnihotri *et al.* 2013, Furtado *et al.* 2015, Mosalam and Günay 2015, Edri and Yankelevsky 2017, Di Trapani *et al.* 2018, Akhoundi *et al.* 2018, among many others). A detailed recent research on OOP strength models was proposed by Pasca *et al.* (2017). In addition, different OOP strength formulations have been proposed. Mechanical-based formulations by McDowell *et al.* (1959) and by Angel *et al.* (1994) were proposed to calculate the strength granted by one-way arching. Also, Eurocode 6 (2004) proposed a very simple mechanical-based formulation for the assessment of the lateral strength of URM walls due to one-way arching. A mechanical-based formulation accounting for two-way arching was proposed by Bashandy *et al.* (1995). Empirical formulations of the OOP strength of infills in which two-way arching occurs were proposed by Dawe and Seah (1989), Flanagan and Bennett (1999) and Ricci *et al.* (2018). The effectiveness of these formulations in predicting the OOP strength of URM infills tested under lateral loading has been already checked in previous works by the Authors of this study (Ricci *et al.* 2018, Di Domenico *et al.* 2018a).

Namely, it has been shown that, for infills in which one-way arching occurs, Eurocode 6 formulation is quite effective while Angel *et al*. (1994)’s formulation seems to be significantly conservative. Clearly, the effectiveness of Eurocode 6 formulation has been evaluated on specimens in which only one-way arching occurs. For the same infills, it

*Corresponding author, Ph.D.
E-mail: mariano.didomenico@unina.it
[a]Associate Professor
E-mail: verderam@unina.it
[b]Assistant Professor
E-mail: paolo.ricci@unina.it

http://www.techno-press.com/journals/sem&subpage=7
ISSN: 1225-4568 (Print), 1598-6217 (Online)

Table 1 Construction materials' mechanical properties

mechanical property	symbol (unit)	boundary condition	80 mm-thick infills mean value	120 mm-thick infills mean value
concrete compressive strength	f_{cm} (N/mm^2)	all	36.0	46.2
steel rebars yielding stress	f_{ym} (N/mm^2)	all	552	497
masonry compressive strength (parallel to holes)	f_{mh} (N/mm^2)	2E	2.45	2.79*
		3E	2.88	
		4E	2.21	2.12
masonry compressive strength (perpendicular to holes)	f_{mv} (N/mm^2)	2E	1.81	2.21
		3E	2.44	
		4E	1.80	1.65
masonry elastic modulus (parallel to holes)	E_{mh} (N/mm^2)	2E	1255	1752**
		3E	2502	
		4E	1188	1262
masonry elastic modulus (perpendicular to holes)	E_{mv} (N/mm^2)	2E	1090	1770
		3E	1846	
		4E	1517	1455

*: This value has been obtained as the product of f_{mv} times the mean of the f_{mh}/f_{mv} ratios of the entire dataset reported in the table.

**: This value has been obtained as the product of f_{mh} and the mean of the E_{mh}/f_{mh} ratios of the entire dataset reported in the table.

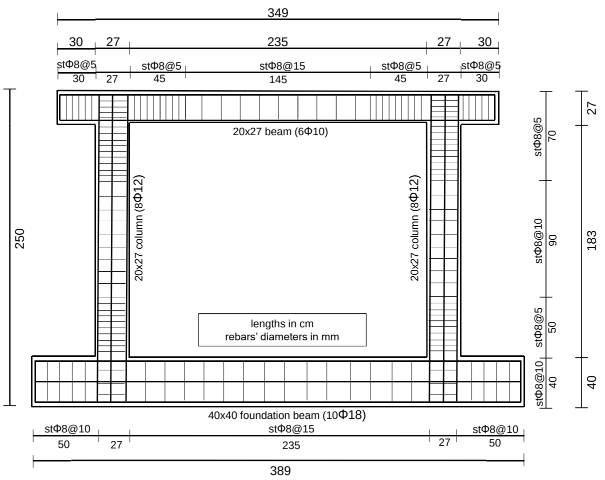

Fig. 1 Construction drawings of the RC frame specimen

Fig. 2 Picture of a specimen

was observed that Angel *et al.* (1994)'s formulation is conservative. So, it can be concluded that both Eurocode 6's formulation and Angel *et al.* (1994)'s formulations should be even more conservative for URM infills in which two-way arching occurs. For this reason, these formulations are adequate for a code-based approach to the seismic safety check of infills. Actually, no specific formulation for URM infills' OOP strength can be found in Eurocodes. For this reason, the practitioner seems to be expected to use Eurocode 6's formulation not only for URM walls (one-way arching) but also for URM infills (two-way arching). On the other hand, Angel *et al.* (1994)'s formulation (in some cases in a simplified and even more conservative version) is proposed by different American standards (such as FEMA 306 1998, FEMA 356 2000 and ASCE/SEI 41-13).

For infills in which two-way arching occurs, it has been shown that Flanagan and Bennett's empirical formulation, which is a slightly modified and simplified version of Dawe and Seah's relationship, is significantly conservative. Therefore, also this formulation is adapt to a code-based safety check of URM infills and, in fact, is suggested for this aim by the New Zealand guidelines to the seismic assessment of buildings (NSZEE 2017).

Clearly, the characterization and prediction of the OOP strength of URM infills is probably the first and most important issue that must be investigated, and further experimental and theoretical efforts are certainly needed on this topic. Consider also that URM infill walls are widespread in RC buildings in the Mediterranean area and that recent earthquakes showed that they are significantly prone to OOP seismic accelerations. These accelerations can produce their collapse, which is highly dangerous for human life safety.

However, modelling the complete OOP force-displacement response of such panels is still an open issue that deserves adequate attention and investigation with the aim of providing, in the future, increasingly complete, robust and reliable indications for their seismic assessment and safety check. In this regard, Dawe and Seah proposed i) an empirical formulation for the prediction of OOP strength, and ii) a mechanical model, based on the application of the Principle of Virtual Works, aimed at predicting the entire OOP force-displacement response. Dawe and Seah's model allows accounting for the formation of one-way (horizontal or vertical) or two-way (both horizontal and vertical) arching action, as well as for the effective boundary conditions at the edges of the infill and for the effect of the confining structural elements' deformability on the OOP behaviour of the confined infill panel.

The first scope of this paper is defining a complete, clear and immediately usable framework for the application of Dawe and Seah's model. To this aim, the defined framework is also applied to compare the predicted force-displacement curve with the experimental response registered for six specimens tested in the laboratory of the Department of Structures for Engineering and Architecture of the University of Naples Federico II (DIST-UNINA).

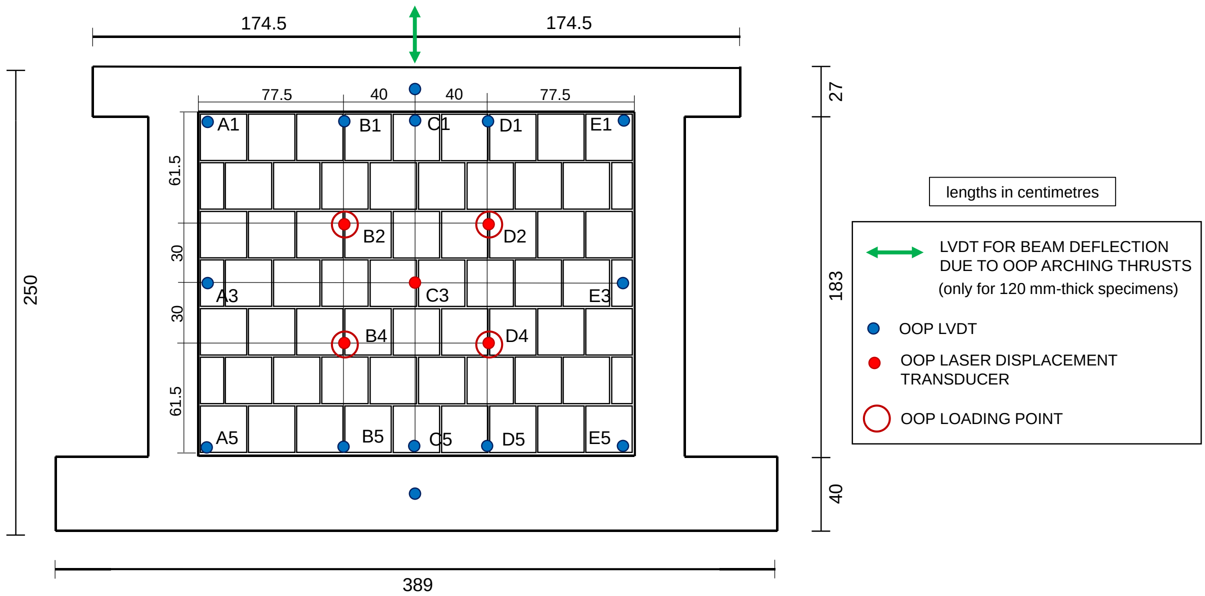

Fig. 3 Loading points' position and instrumentation layout

The results of the comparison are used to assess the effectiveness of the model, to enlighten its strengths and to discuss its weaknesses and possible modifications.

To achieve all these goals, the paper is structured as it follows. First, the experimental program carried out at DIST-UNINA is described and the main results obtained are summarized. Second, the mechanical principles on which Dawe and Seah's model is based are recalled and the model itself is described in detail. Third, the model is applied with reference to the infill walls tested at DIST-UNINA and the results of this application are compared with the experimental response of test specimens. Finally, the results of the comparison are discussed.

2. Experimental program description and tests' results

This section is dedicated to the general description of the experimental program carried out at DIST-UNINA. The testing procedure is presented and test specimens' characteristics and materials' properties are described, as well as the instrumentation layout and the loading system used to carry out tests. Further details can be found in Di Domenico *et al.* (2018a). In addition, the results of tests are summarized. Further discussion on these results can be found in Di Domenico *et al.* (2018a, b).

2.1 Experimental program general description

The tests herein described were carried out on six test specimens equal for geometric and nominal mechanical properties, except for their thickness. Namely, two sets constituted by three 2:3 scaled URM infill walls in RC frames were tested. The infills of the first set (80_ specimens) were 80 mm thick. The infills of the second set (120_specimens) were 120 mm thick. As the height of the

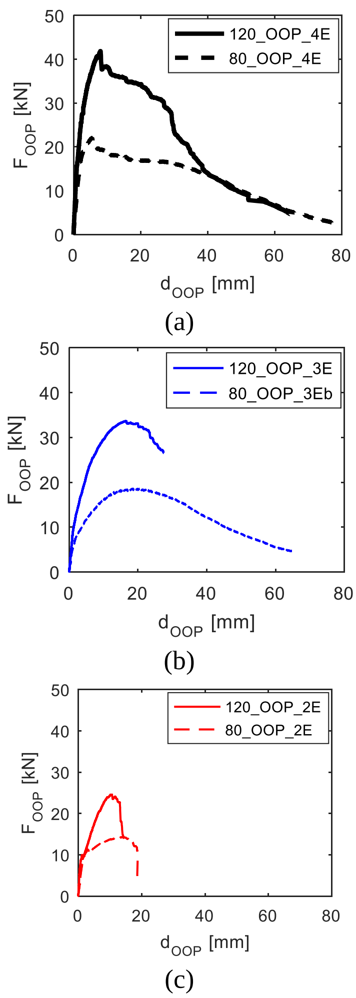

Fig. 4 Experimental response of the specimens bounded along four (a) three (b) and two (c) edges

infills was always equal to 1830 mm, the height-over-thickness slenderness ratio for the infills of the first set was

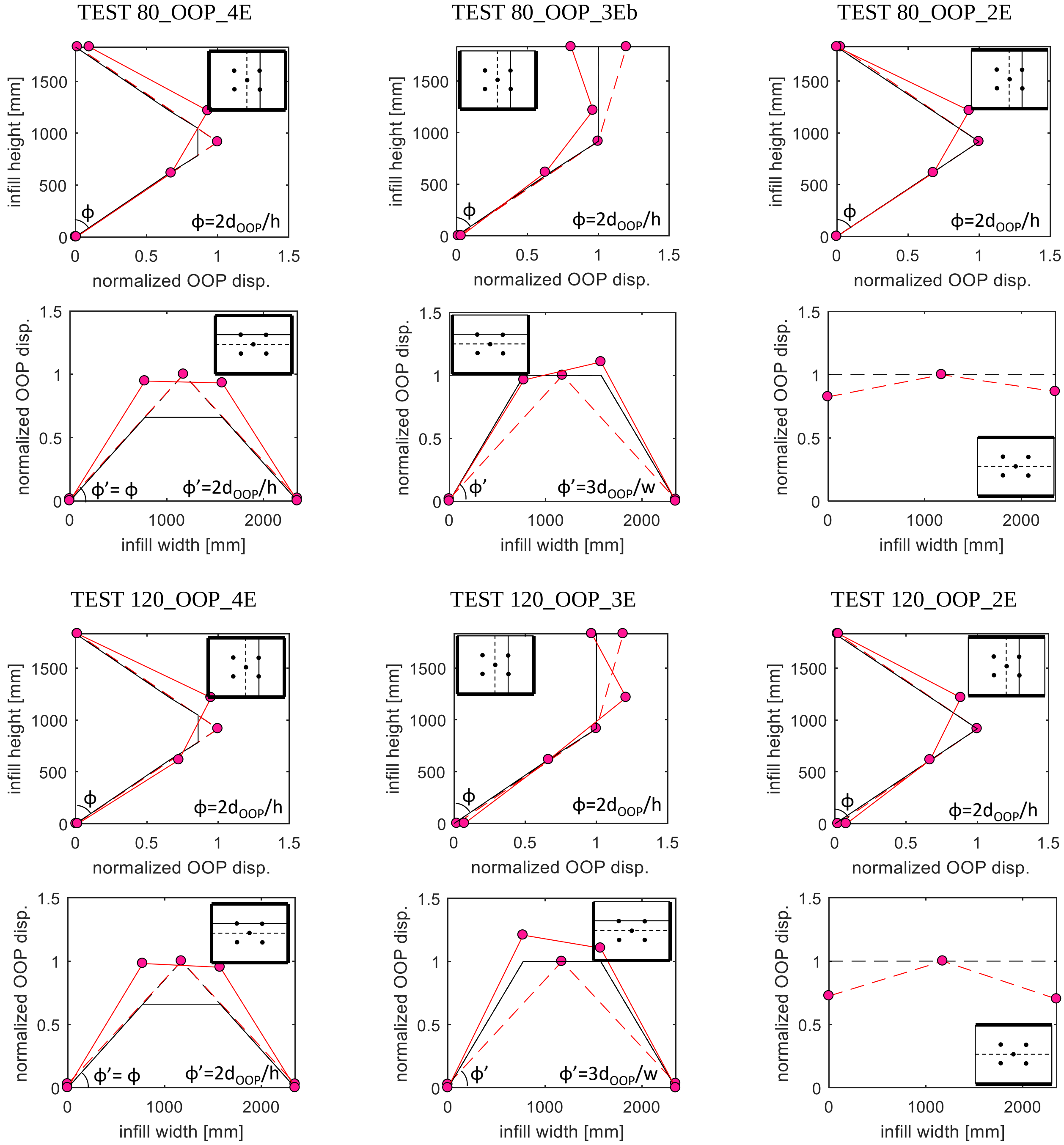

Fig. 5 Experimental deformed shapes at the attainment of peak load for test specimens (red lines) together with their regularized form used for the application of Dawe and Seah's model (black lines)

equal to 22.9, while it was equal to 15.2 for the second set. For each set, three different boundary conditions at edges were investigated: one infill was mortared to confining frame along the upper and the lower edges, i.e., was bounded to the confining frame along two edges (OOP_2E specimens); one infill was bounded to the confining frame along the lower and both the lateral edges, i.e., was bounded to the confining frame along three edges (OOP_3E specimens); finally, one infill was bounded to the confining frame along all the edges (OOP_4E specimens). Clearly, in "2E" specimens only one-way vertical arching can occur; in "3E" specimens, only one-way horizontal arching can occur; in "4E" specimens, two-way horizontal and vertical arching can occur. Note that, for consistency with previous works by the Authors, the 80 mm-thick specimen bounded along three edges will be herein called 80_OOP_3Eb specimen.

The 2:3 scaled RC frames were designed according to the seismic Italian building code NTC2008 (2008). Construction drawings of the RC frame, with geometric and reinforcement details are reported in Fig. 1. A picture of a test specimen is reported in Fig. 2. Infill walls with 80 mm and 120 mm thickness were realized by using 250×250 mm^2 clay hollow bricks placed with horizontal holes and 1 cm thick horizontal and vertical courses of class M5 mortar. Construction materials' mean mechanical properties are reported in Table 1. The compressive strength of concrete was determined on 150×150×150 mm^3 cubes according to the European standard EN 206-1 while the tensile strength of steel rebars was determined on 1000 mm long specimens according to the European standard EN 10080. Masonry compressive strength and elastic modulus were determined by vertical and horizontal compression tests on 770×770×80 mm^3 masonry wallets, according to EN 1052-1 standard.

OOP loads were applied on four points by means of spherical hinges. The loading points are placed on the infill's diagonals, as shown in Fig. 3. The same loading system was used for similar tests by Calvi and Bolognini (2001) and Guidi *et al.* (2013). No axial load was applied on columns.

As shown in Fig. 3, twelve LVDTs (Linear Variable Displacement Transducers) were placed along the infills' edges to read OOP displacements due to a potential detachment of the infill from the surrounding frame. Five laser displacement transducers were placed to read OOP displacements of the infill centre and of the four loading points. Two LVDTs were placed at the centre of the RC frame upper and foundation beam, in order to read potential OOP translation or drifts of the RC frame during tests. Only for the tests on the 120 mm-thick infills, a vertical LVDT was placed at the centre of the upper beam upper edge to read potential deflections of the beam due to arching thrusts. The OOP load was applied in displacement control with OOP displacements monotonically increasing at 0.02 mm/s velocity.

2.2 General considerations on tests' results

The OOP response of specimens is compared in Fig. 4. As expected, for all boundary conditions, the OOP strength exhibited by thicker infills is greater than that observed for slender infills. In addition, the strength of specimens in which two-way arching occurs is greater than that of specimens in which only one-way arching occurs. It can also be observed that the strength of specimens in which one-way horizontal arching occurs is greater than that provided by one-way vertical arching. This is due, in this specific case, to masonry mechanical properties (as shown in Table 1), despite the infill aspect ratio. In reference to the general response of specimens, it can be noted that, independently on the specimens' slenderness, the response of infills with equal boundary conditions is similar. Namely, infills bounded along two edges showed a load-bearing capacity drop soon after the attainment of peak load. This is due, most likely to masonry crushing due to vertical arching thrusts. Masonry crushing is brittle when masonry is loaded perpendicular to bricks' holes (Di Domenico *et al.* 2018b), as in this case. Given that, the brittle failure of infills is also due to the absence of a number of restrained edges adequate to allow stresses redistribution after masonry vertical crushing. On the contrary, infills bounded along three and four edges showed a non-negligible post-peak displacement capacity. This is due to the redistribution of stresses occurring after peak load towards the specimens' lateral edges combined with the post-peak deformation capacity of masonry loaded by horizontal arching thrusts parallel to bricks' holes (Di Domenico *et al.* 2018b).

As it will be useful for Dawe and Seah's model application, the deformed shapes of test specimens at the attainment of peak load are shown in Fig. 5. Such deformed shapes, represented along some vertical and horizontal alignments, are obtained through the displacements read by instruments placed as shown in Fig. 3. The experimental deformed shapes, with displacements normalized with respect to the OOP displacement of the infill centre, d_{OOP}, are represented with red lines.

As will be described in detail in section 3, it is necessary for the application of Dawe and Seah's model to define a regularized "reference" deformed shape for each specimen. The abovementioned regularized and idealized deformed shapes have been defined based on the experimental ones shown in Fig. 3 and are represented, together with the experimental ones, in the same figure with a black line. Further details on this topic are provided in section 3.

3. Dawe and Seah's OOP response model

In this section, Dawe and Seah's model is applied to obtain theoretical predictions of the entire force-displacement response for all specimens and compare them to their experimental response. The model is based on the application, for increasing values of the infill OOP central displacement, of the equation of virtual works by means of fracture line analysis.

A fracture line is a large crack that defines, together with other large cracks, a cracking pattern that allows considering the infill as constituted by separate parts rigidly rotating around them. Note that the "effective" cracking pattern considered in the application of Dawe and Seah's stripe procedure is not necessarily consistent with the entire "actual" cracking pattern observed during experimental tests. In fact, the "effective" cracking pattern that is considered and idealized must be consistent with the deformed shape shown by the infill wall under lateral OOP load. This is a fundamental point, as moments that work for the rigid rotations of the infill parts defined by the "effective" cracking pattern are calculated, step-by-step, based on the deformed shape of the infill. If moments associated with masonry flexural strength are considered when calculating the internal virtual work, the OOP strength of the infill can be highly underestimated (Brincker 1984).

However, if arching action occurs, moments acting along fracture lines overcome those associated with masonry flexural strength, which depends on masonry tensile strength, and their value is defined by masonry compressive strength. Namely, moments associated with arching action depend on the compressive stresses acting in the infill thickness due to arching thrusts formed in the wall thickness and on their lever arm, as will be shown in the following. As this lever arm depends on the deformed shape of the infill, the moment acting along fracture lines varies at increasing OOP central displacement, as well as along

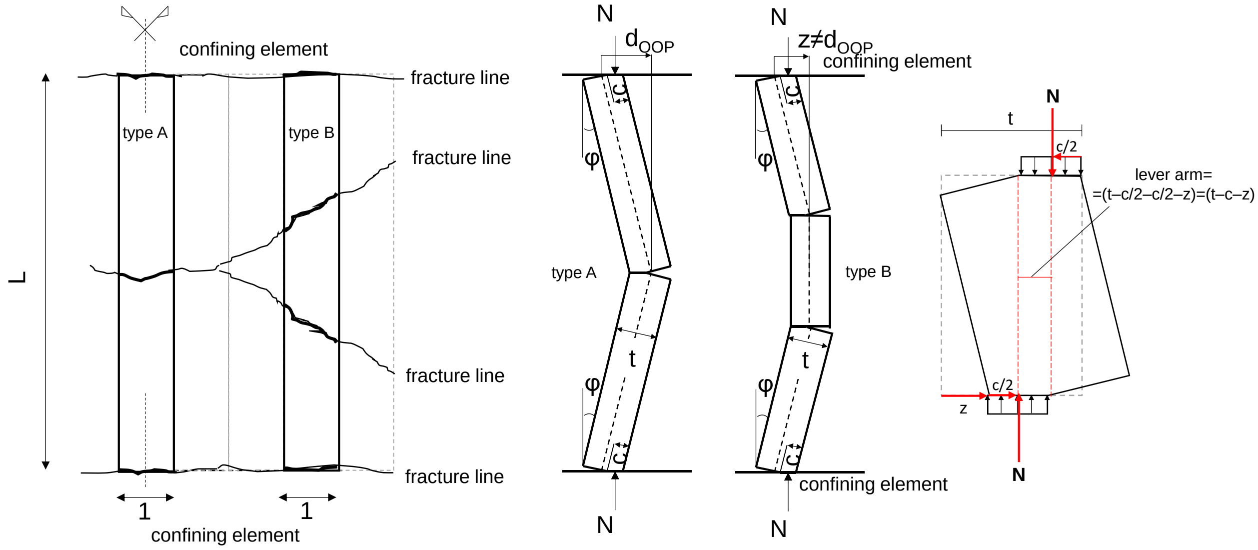

Fig. 6 Deformed shape of a type A and type B stripes divided by fracture lines in separate parts rigidly rotating about their ends. On the right, a particular of a stripe single part

fracture lines themselves. To account for this double variation, fracture line analysis is usually applied by discretizing infill walls into vertical and horizontal non-interacting stripes. Vertical stripes allow accounting for vertical thrusts and moments along fracture lines associated with them; horizontal stripes allow accounting for horizontal thrusts and moments along fracture lines associated with them.

In this section, first, the main principles and hypotheses of Dawe and Seah's stripe method are recalled briefly. Then, the deformed shape of test specimens is described and fixed, separately for each one, as "reference deformed shape" for the application of the method.

3.1 Recall on Dawe and Seah's model fundamentals

Consider an infill wall divided in unit-width stripes with length equal to L and subjected to lateral loading. Given an "effective" cracking pattern, each stripe is crossed by one or more fracture lines. As shown in Fig. 6, it is usual considering two types of stripes, as also done in this study. A "type A" stripe is crossed by one fracture line at its centre. Such fracture line separates type A stripes in two equal length parts rigidly rotating around their ends. A "type B" stripe is crossed by two fracture lines, both of them at the same distance from the stripe nearer end. The two fracture lines separate type B stipes in three parts, with the two exterior parts rigidly rotating around their ends. Clearly, if d_{OOP} is the OOP central displacement of the infill, e.g., the central and maximum displacement of a type A stripes, type B stripes have a maximum displacement z which is different from d_{OOP} due to geometric compatibility. Hence, as the infill will be considered as divided in separate parts rigidly rotating around fracture lines, the reference deformed shape defined for the application of the method is a linear relation among z (OOP maximum displacement of the generic stripe) and d_{OOP} (OOP central displacement of the infill).

At a certain value of z, a certain rotation φ is defined for each stripe, as reported in Eq. (1).

$$\varphi = \frac{2z}{L} \tag{1}$$

At increasing d_{OOP} (and, therefore, for each stripe, at increasing z and φ), increasing compressive stresses develop at the ends of each stripe part. Such compressive stresses produce arching thrusts opposite in their horizontal component to the external load. The compressive stresses develop along the contact length between the masonry segment and the confining elements. The contact length (or neutral axis depth), c, is calculated as reported in Eq. (2), which has been derived by Dawe and Seah based on compatibility and equilibrium conditions.

$$c = \frac{2t\tan\varphi - L(1-\cos\varphi)}{4\tan\varphi + (k_1 k_2 f_m L/tE_m)\cos\varphi} \tag{2}$$

In Eq. (2), k_1 and k_2 are stress block parameters both set to 0.85, f_m and E_m are masonry compressive strength and elastic modulus, respectively, in the direction examined.

According to Dawe and Seah, the resultant of compressive stresses acting, per unit length, in the depth of contact is equal to N, which is calculated as reported in Eq. (3).

$$N = k_1 k_2 f_m c \tag{3}$$

This force acts at a distance equal to 0.5c from the outermost compressed fibre of the stripe cross-section. Note that, through c, N depends only on the rotation, which is equal for all stripes, and on the infill geometric and mechanical properties. As shown in Fig. 6, N generates a moment with respect to the stripe cross section centroid which is calculated as reported in Eq. (4).

$$M = 0.5N(t-c-z) \tag{4}$$

Note that the moment depends on the OOP maximum displacement of the considered stripe, so it varies for each stripe, as already stated. For each value of d_{OOP}, z can be calculated for all stripes as a reference deformed shape has been defined, φ can be calculated through Eq. (1), c through Eq. (2), N through Eq. (3) and M through Eq. (4). The internal work for each infill stripe is calculated as reported in Eq. (5).

$$L_{I,stripe} = 2N(t-c-z)\varphi = 4N(t-c-z)\frac{d_{OOP}}{L} \quad (5)$$

Given a certain value of the OOP central displacement d_{OOP}, the sum of the internal works calculated for both horizontal and vertical stripes must be calculated and equated to the external work. This equation provides the OOP force corresponding to the fixed OOP central displacement d_{OOP} and, so, the OOP force-displacement curve for the considered infill.

All the above described approach can be applied also when considering the presence of a gap g between the infill confining elements and the infill edges (as for "3E" and "2E" specimens) To account for this, only Eq. (2) should be modified as reported in Eq. (6).

$$c = \frac{2t\tan\varphi - L(1-\cos\varphi) - g}{4\tan\varphi + (k_1 k_2 f_m L/tE_m)\cos\varphi} \quad (6)$$

Note that g is assumed as a constant, i.e., is equal to the initial gap existing between the infill wall and the confining elements.

Eq. (6) can be modified to consider also the deformability of the confining frame elements. In fact, due to arching thrusts, the structural elements that support infills deform and it is possible to associate with each stripe the total outward displacement of the confining elements (i.e., the sum of the outward displacements calculated at each end of the stripe), f, in correspondence with the considered stripe. To account for this, only Eq. (6) should be modified as reported in Eq. (7).

$$c = \frac{2t\tan\varphi - L(1-\cos\varphi) - g - f}{4\tan\varphi + (k_1 k_2 f_m L/tE_m)\cos\varphi} \quad (7)$$

Differently from g, f is a function of d_{OOP}, as at increasing OOP central displacement arching thrusts vary and, so, also the outward displacement of the confining frame elements, which is subjected to arching thrusts applied by the infill, varies. Note that, as f is different for each stripe, when the deformability of the confining frame is considered, the depth of contact c is different for each stripe, and, therefore, also N is different for each stripe. In other words, when the infill is confined by stiff elements, the vertical and/or horizontal arching thrusts are uniformly distributed along its width/height. On the contrary, if the confining elements are deformable, such thrusts are no more uniformly distributed and are lower where the confining elements maximum deflections are expected.

3.2 Evaluation of the reference deformed shape of test specimens

As already stated and shown through Eqs. (4)-(5), a reference deformed shape has to be defined to apply Dawe and Seah's stripe method. In other words, a linear relationship between the OOP central displacement, d_{OOP}, and the OOP displacement at a generic point of the infill wall, z, must be chosen. In the application of the procedure, i.e., at increasing values of d_{OOP}, this relation cannot vary, even if this is not perfectly consistent with reality and experimental evidences.

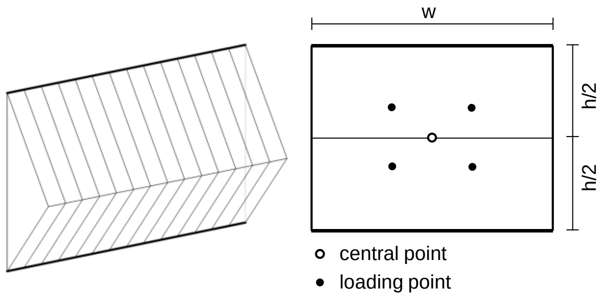

Fig. 7 Reference deformed shape for specimens 80_OOP_2E and 120_OOP_2E

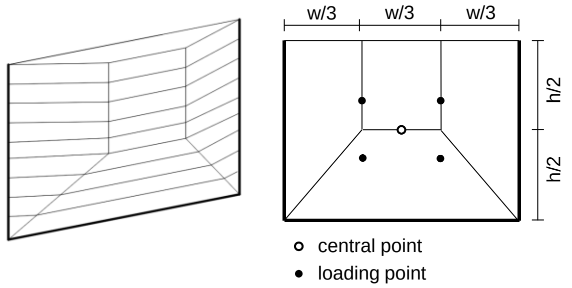

Fig. 8 Reference deformed shape for specimens 80_OOP_3Eb and 120_OOP_3E

For the applications herein proposed, a regularized reference deformed shape will be defined for all specimens, based on the experimental data read by instruments in correspondence of the peak load point. This is an assumption and is based on the predominant significance, of course, of the peak load point among all the force-displacement couples that define the OOP response of specimens.

A very simple assumption can be made when dealing with 80_OOP_2E and 120_OOP_2E specimens. In fact, in these cases, the deformed shape at peak load reported in Fig. 5 can be idealized and regularized in accordance with the deformed shape shown in Fig. 7. Both vertical and horizontal stripes are considered. However, in this case, the value of c calculated by means of Eq. (6) for horizontal stripes is always negative. This means that arching action in the horizontal direction cannot occur, as expected. So, horizontal stripes do not contribute to the definition of the internal work and only vertical stripes (i.e., vertical arching) should be considered.

The total external work, based on the reference deformed shape shown in Fig. 7, is reported in Eq. (8).

$$L_E = \frac{F}{4}\frac{2d_{OOP}}{3} + \frac{F}{4}\frac{2d_{OOP}}{3} + \frac{F}{4}\frac{2d_{OOP}}{3} + \frac{F}{4}\frac{2d_{OOP}}{3} = \frac{2}{3}Fd_{OOP} \quad (8)$$

Consider now specimens 80_OOP_3Eb and

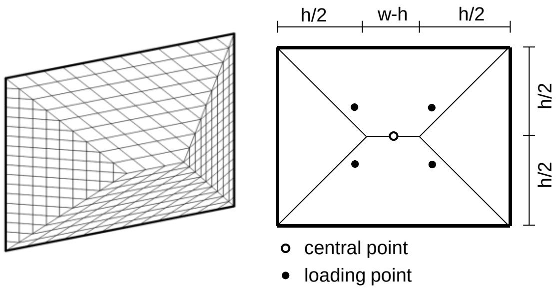

Fig. 9 Reference deformed shape for specimens 80_OOP_4E and 120_OOP_4E

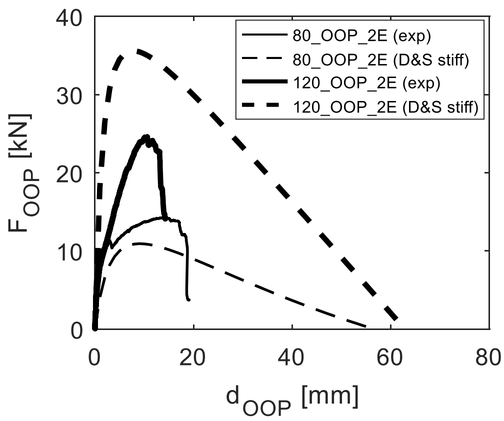

Fig. 10 Comparison between the OOP force-displacement relationship predicted by Dawe and Seah under the hypothesis of stiff confining elements with the experimental response for specimens 80_OOP_2E and 120_OOP_2E

120_OOP_3E and their deformed shapes at peak load shown in Fig. 6. Remembering that the reference deformed shape is somehow idealized and regularized, it seems reasonable to assume for both specimens that points B1, C1, D1, the loading points B2 and D2 and the central point C3 (see the instruments layout in Fig. 3) have the same displacement. The reference deformed shape shown in Fig. 8 is considered. In this case, both vertical and horizontal stripe are considered and Eq. (6) is applied for the calculation of the compression depth c for vertical stripes. However, the presence of a top gap g neutralizes the contribution of the internal work associated with vertical stripes. Hence, actually, only horizontal arching occurs and contributes to the specimens' OOP load-bearing capacity.

The total external work, based on the reference deformed shape shown in Fig. 8, is reported in Eq. (9).

$$L_E = \frac{F}{4}d_{OOP} + \frac{F}{4}d_{OOP} + \frac{F}{4}\frac{2d_{OOP}}{3} + \frac{F}{4}\frac{2d_{OOP}}{3} = \frac{5}{6}Fd_{OOP} \tag{9}$$

For specimens 80_OOP_4E and 120_OOP_4E, the deformed shapes at peak load are shown in Fig. 5. Remembering that the reference deformed shape is somehow idealized and regularized, it seems reasonable to assume for both specimens that the four loading points have the same displacement while the central point has a higher displacement. In addition, considering the slope of the dashed lines in Fig. 5, it seems reasonable to assume that the deformed shape is provided of a horizontal "ridge line", as shown in Fig. 9 that reports the reference deformed shape for both specimens. In this case, both vertical and horizontal stripes are considered and Eq. (2) is applied for the calculation of the compression depth c. Both vertical and horizontal arching occur and contribute to the specimens' OOP load-bearing capacity.

The total external work, based on the reference deformed shape shown in Fig. 9, is reported in Eq. (10).

$$L_E = \frac{F}{4}\frac{2d_{OOP}}{3} + \frac{F}{4}\frac{2d_{OOP}}{3} + \frac{F}{4}\frac{2d_{OOP}}{3} + \frac{F}{4}\frac{2d_{OOP}}{3} = \frac{2}{3}Fd_{OOP} \tag{10}$$

4. Application of Dawe and Seah's model on test specimens under the hypothesis of stiff boundary elements

First, Dawe and Seah's stripe method is applied under the hypothesis of stiff confining elements. This means that the procedure described in section 3 is applied by calculating the compression-bearing width, c, by means of Eq. (6).

The application is very simple for "2E" specimens. In that case, the total internal work associated only with vertical stripes and obtained by integrating Eq. (5) on the entire infill width is reported in Eq. (11).

$$L_I = 4N_v d_{OOP}(t - c_v - d_{OOP})\frac{w}{h} \tag{11}$$

In Eq. (11), the v subscript indicates that the arching thrust N and the contact depth c are calculated with reference to vertical arching. By equating the total internal work (Eq. (11)) and the external work (Eq. (8)), the relationship between the OOP four-point load, F, with the OOP central displacement, d_{OOP}, is obtained. This relationship, indicated as $F(d_{OOP})$, is reported in Eq. (12).

$$F(d_{OOP}) = 6N_v(t - c_v - d_{OOP})\frac{w}{h} \tag{12}$$

The results of Eq. (12) are compared with the experimental force-displacement response of specimens 80_OOP_2E and 120_OOP_2E in Fig. 10.

For specimen 80_OOP_2E, the OOP strength is underestimated (10.9 kN vs an observed strength equal to 14.6 kN), while for specimen 120_OOP_2E the strength is significantly overestimated (35.6 kN vs an observed value of 24.0 kN). In addition, the theoretical model fails in predicting the entire post-peak behaviour of specimens and their sudden failure.

For "3E" specimens in stiff RC members, the total internal work associated only with horizontal stripes is reported in Eq. (13b), which has been obtained by integrating Eq. (13a) on the entire infill height. Note that the internal work associated with vertical stripes is null due to the gap g between the infill upper edge and the RC frame

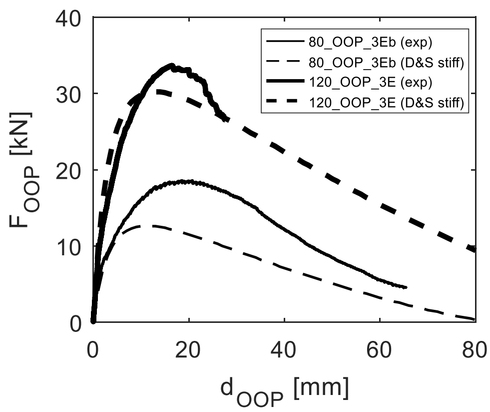

Fig. 11 Comparison between the OOP force-displacement relationship predicted by Dawe and Seah under the hypothesis of stiff confining elements and the experimental response for specimens 80_OOP_3Eb and 120_OOP_3E

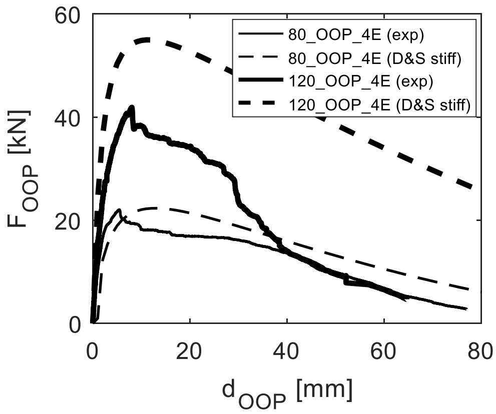

Fig. 12 Comparison between the OOP force-displacement relationship predicted by Dawe and Seah under the hypothesis of stiff confining elements and the experimental response for specimens 80_OOP_4E and 120_OOP_4E

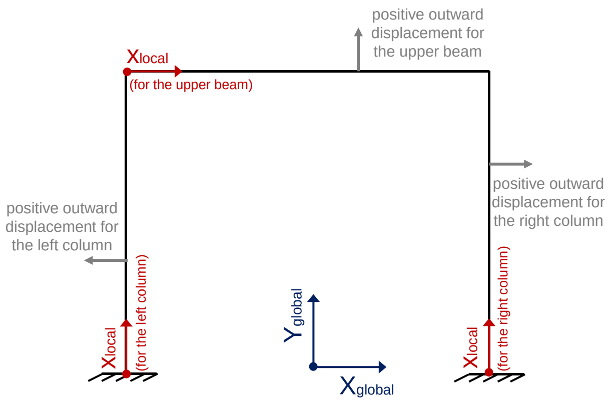

Fig. 13 Conventions on the reference global and local axes and signs adopted

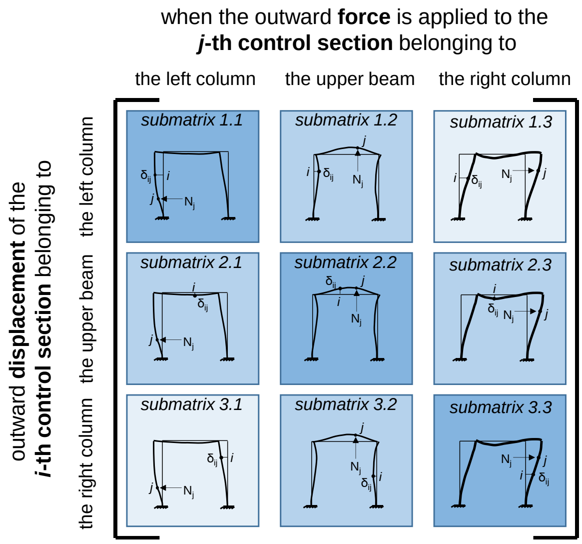

Fig. 14 Partitioned deformability matrix

upper beam.

$$L_{I,stripe} = 6N_h(t - c_h - z)\frac{d_{OOP}}{w} \quad (13a)$$

$$L_I = \left[6N_h\frac{h}{w}(t - c_h) - \frac{9}{2}N_h\frac{h}{w}d_{OOP}\right]d_{OOP} \quad (13b)$$

In Eqs. (13a)-(13b), the h subscript indicates that the arching thrust N and the contact depth c are calculated with reference to horizontal arching. By equating the total internal work reported in Eq. (13b) with the external work reported in Eq. (9), the relationship between the OOP four-point load F with the OOP central displacement d_{OOP} is obtained and reported in Eq. (14).

$$F(d_{OOP}) = \frac{9}{5}N_h\frac{h}{w}[4(t - c_h) - 3d_{OOP}] \quad (14)$$

The results of Eq. (14) are compared with the experimental force-displacement response of specimens 80_OOP_3Eb and 120_OOP_3E in Fig. 11.

For specimen 80_OOP_3Eb, the OOP strength is significantly underestimated (12.7 kN vs an observed strength equal to 18.4 kN), while for specimen 120_OOP_3E the strength is slightly underestimated (30.2 kN vs an observed value of 33.6 kN).

Consider now "4E" specimens. In this case, the total internal work is reported in Eq. (15).

$$\begin{aligned} L_I = 8d_{OOP}[N_v(t - c_v) - N_v d_{OOP}]\left(\frac{w - h}{h}\right)d_{OOP} \\ + [4N_v(t - c_v) - 2N_v d]d_{OOP} \\ + [2N_h(t - c_h) - N_h d_{OOP}] \end{aligned} \quad (15)$$

By equating the total internal work (Eq. (15)) and the external work (Eq. (10)), the relationship between the OOP load, F, with the OOP central displacement is obtained. The relationship is reported in Eq. (16).

$$\begin{aligned} F(d_{OOP}) = 6N_v(t - c_v)\frac{w}{h} - 6N_v\left(\frac{w}{h} - 1\right)d \\ - 3N_v d_{OOP} + 6N_h(t - c_h) \\ - 3N_h d_{OOP} \end{aligned} \quad (16)$$

The results of Eq. (16) are compared with the experimental force-displacement response of specimens

Table 2 Values of δ_{ij} for the deformability matrix. In the following Equations, $a=EI_b/EI_c$ and $b=w/h$. EI_b and EI_c are the flexural stiffness of the beam and of the columns' cross sections, respectively

submatrix 1.1		
$\frac{(x_i^2(-2(6a+b)(a+2b)h^3x_i+6(6a+b)(a+2b)h^3x_j+3h(-(15a^2+26ab+3b^2)h+(a+b)(6a+b)x_i)x_j{}^2+(6a+b)(3(a+b)h-(2a+b)x_i)x}{(12(6a+b)(a+2b)EI_ch^3)}$	$x_i \leq x_j$	(18)
$\frac{(x_j{}^2(3hx_i(2(6a+b)(a+2b)h^2-(15a^2+26ab+3b^2)hx_i+(a+b)(6a+b)x_i^2)-(6a+b)(2(a+2b)h^3-3(a+b)hx_i^2+(2a+b)x_i^3)x_j))}{(12(6a+b)(a+2b)EI_ch^3)}$	$x_i > x_j$	(19)
submatrix 1.2		
$\frac{x_i^2(bh-x_j)x_j(b(b(h+x_i)+a(-5h+6x_i))-2(a+2b)x_j)}{4b(6a+b)(a+2b)EI_ch^2}$		(20)
submatrix 1.3		
$\frac{(x_i^2x_j{}^2(3h(-(9a^2+14ab+3b^2)h+(a+b)(6a+b)x_i)+(6a+b)(3(a+b)h-(2a+b)x_i)x_j))}{(12(6a+b)(a+2b)EI_ch^3)}$		(21)
submatrix 2.1		
$\frac{(bh-x_i)x_ix_j{}^2(a(-5bh-2x_i+6bx_j)+b(-4x_i+b(h+x_j)))}{4b(6a+b)(a+2b)EI_ch^2}$		(22)
submatrix 2.2		
$\frac{-(x_i(bh-x_j)(2b(6a+b)(a+2b)h^2x_i^2-bh(3ab(8a+5b)h^2+3b(13a+4b)hx_i-2(a+2b)x_i^2)x_j+2(a+2b)(6abh^2+(3bh-2x_i)x_i)x_j{}^2))}{(12ab^2(6a+b)(a+2b)EI_ch^3)}$	$x_i \leq x_j$	(23)
$\frac{((bh-x_i)x_j(3abh^2x_i(b(8a+5b)h-4(a+2b)x_i)+3bhx_i(b(13a+4b)h-2(a+2b)x_i)x_j-2(a+2b)(b(6a+b)h^2+bhx_i-2x_i^2)x_j{}^2))}{(12ab^2(6a+b)(a+2b)EI_ch^3)}$	$x_i > x_j$	(24)
submatrix 2.3		
$\frac{-(bh-x_i)x_ix_j{}^2(7abh+3b^2h-2ax_i-4bx_i-b(6a+b)x_j)}{4b(6a+b)(a+2b)EI_ch^2}$		(25)
submatrix 3.1		
$\frac{(x_i^2x_j{}^2(3h(-(9a^2+14ab+3b^2)h+(a+b)(6a+b)x_i)+(6a+b)(3(a+b)h-(2a+b)x_i)x_j))}{(12(6a+b)(a+2b)EI_ch^3)}$		(26)
submatrix 3.2		
$\frac{(x_i^2(bh-x_j)x_j(a(-7bh+6bx_i+2x_j)+b(b(-3h+x_i)+4x_j)))}{(4b(6a+b)(a+2b)EI_ch^2)}$		(27)
submatrix 3.3		
$\frac{(x_i^2(-2(6a+b)(a+2b)h^3x_i+6(6a+b)(a+2b)h^3x_j+3h(-(15a^2+26ab+3b^2)h+(a+b)(6a+b)x_i)x_j{}^2+(6a+b)(3(a+b)h-(2a+b)x_i)x}{(12(6a+b)(a+2b)EI_ch^3)}$	$x_i \leq x_j$	(28)
$\frac{(x_j{}^2(3hx_i(2(6a+b)(a+2b)h^2-(15a^2+26ab+3b^2)hx_i+(a+b)(6a+b)x_i^2)-(6a+b)(2(a+2b)h^3-3(a+b)hx_i^2+(2a+b)x_i^3)x_j))}{(12(6a+b)(a+2b)EI_ch^3)}$	$x_i > x_j$	(29)

80_OOP_4E and 120_OOP_4E in Fig. 12.

For specimen 80_OOP_2E, the OOP strength is perfectly caught (22.3 kN vs an observed strength equal to 22.0 kN), while for specimen 120_OOP_2E the strength is significantly overestimated (55.0 kN vs an observed value of 41.9 kN).

Prior to whichever consideration on the quality of the performances of Dawe and Seah's model, it is worth to remember that the model itself allows accounting for the deformability of the surrounding elements and for its influence on the entity of arching thrusts and, so, on the OOP strength/response of specimens. This issue is investigated in the following section. Clearly, as pointed out by Flanagan and Bennett, the effect of the frame elements deformability can be neglected when dealing with infill walls in a real building. In fact, in this case, the outward deflection of the structural elements confining a certain infill wall is prevented by the presence of other infill walls. However, it will be shown in the next section that the effect of frame elements' deformability cannot be neglected when interpreting experimental tests' results in which the frame elements are not surrounded and "confined" by other infills.

5. Application of Dawe and Seah's model on test specimens under the hypothesis of deformable boundary elements

In this section, Dawe and Seah's model is applied under the hypothesis of deformable confining elements. This means that the procedure described in section 3 is applied by calculating the compression-bearing width, c, by means of Eq. (7).

Remember that, in this case, the contact length c depends, for each stripe, on the total outward displacement of the RC frame beam and columns. In other words, c_v depends on the outward displacement of the upper beam, while c_h depends on the summation of the outward displacements of both columns. The beam outward displacement is assumed as positive when it has the same direction of vertical thrusts, while columns' outward displacements are assumed as positive when they have the same direction of horizontal thrusts acting on each element, as shown in Fig. 13.

Remember that outward displacements evolves at increasing OOP central displacement. In addition, they are different for each stripe. This means that the compression-bearing width, which is calculated by means of Eq. (7), is different for each stripe, as the f term is different for each stripe. As explained by Dawe and Seah themselves and herein recalled, when introducing the frame deformability in the model, it is necessary to implement an iterative procedure to calculate, for each stripe, the correct value of c corresponding to a certain value of d_{OOP}.

The steps of the iterative procedure are the following:

i. The OOP force-displacement must be calculated under the hypothesis of stiff confining elements. For a specific value of d_{OOP}, this leads to a distribution of arching thrusts N acting on the confining structural elements. As already stated, at this stage N is equal for all stripes with the same direction. Therefore, a uniformly distributed outward load acts on the RC frame structural elements.

ii. To introduce the frame deformability in the OOP response model, it is necessary to calculate the frame deformed shape under the load distribution evaluated at the first step. This leads to the definition of a value of f for each stripe.

iii. A new compression-bearing width value must be calculated for each stripe by means of Eq. (7). Clearly, this leads to a new distribution of arching thrusts, which is no more uniform even when associated with stripes with the same direction.

iv. The new outward load distribution leads to a new deformed shape of the confining frame, which leads to a new value of c for all stripes and, so, to a new distribution of arching thrusts.

Steps iii. and iv. should be reiterated until no significant variation in the value of arching thrusts is observed between successive iterations. As this iterative procedure must be performed for each value of d_{OOP}, when accounting for the frame deformability it is not possible to provide a closed-form final relationship between the OOP force and the OOP central displacement. So, in this case, the OOP force-displacement relationship is found numerically: the higher the number of vertical and horizontal stripes, the lower the error made in the discretization of the infill wall in stripes.

5.1 Definition of the confining frame deformability matrix

To achieve all these goals, it is necessary to introduce in the routine a matrix containing the deformability coefficients of the RC frame, Δ. If *n* is the number of horizontal stripes and *m* is the number of vertical stripes, the RC frame elements' outward displacements must be calculated in *n* control sections of each column and in *m* control sections in the upper beam. Each control section corresponds to the centre of a stripe. For all these reasons, the deformability matrix that must be implemented is a square matrix with (*2n+m*) rows and (*2n+m*) columns. The value of n and m can be set by the analyst at will. The generic term of the Δ matrix, δ_{ij}, represents the outward displacement in the *i*-th control section when a unit-force with the direction of arching thrusts is applied in the *j*-th control section. For each value of d_{OOP}, for each iteration, the trial value of the arching thrust acting in the *j*-th stripe, N_j, must be multiplied for the *j*-th column of Δ to obtain the outward displacement of all control sections due to N_j.

When this has been done for all columns of Δ, the actual outward displacement in the *i*-th control section, f_i, which enters Eq. (7), is provided by the sum of all $N_j\delta_{ij}$ products, as reported in Eq. (17).

$$f_i = \sum_{j=1}^{2n+m} N_j\,\delta_{ij} \tag{17}$$

To express in a closed form all the δ_{ij} terms, it is convenient to divide Δ in sub-matrices, as shown in Fig. 14. Namely, both rows and columns of the matrix are divided in three groups. The first group is constituted by *n* matrix rows and by *n* matrix columns and is related to the RC frame left column. The second group is constituted by *m* matrix rows and by *m* matrix columns and is related to the RC frame upper beam. The third group is constituted by *n* matrix rows and by *n* matrix columns and is related to the RC frame right column. Therefore, a total of 9 submatrices is defined. For the sake of clarity, they are numbered in Fig. 14. The generic submatrix carries the outward displacement of a control section belonging to the left column/upper beam/right column when a unit-force is applied, in the direction of arching thrusts, to a control section belonging to the left column/upper beam/right column.

The value of δ_{ij} calculated for each submatrix is formulated in Eqs. (18)-(29), which are reported in Table 2. In these Equations, x_i is the abscissa, in local coordinates, of the frame section in which the displacement is calculated; x_j is the abscissa, in local coordinates, of the frame section in which the thrust force is applied.

5.2 Some modelling issues

Dawe and Seah's model has been defined for URM infills in steel frames. So, when dealing with confining elements' deformability issues, they considered the extensional, flexural and torsional deformability of such elements. In the application herein presented, the extensional and torsional deformability of the confining members has been neglected, as shown also through Eqs. (18)-(29). This is due to two main reasons: first, Flanagan and Bennett demonstrated empirically that, even for URM infills in steel frames, the effect of the extensional and torsional deformability of the confining members can be neglected; second, the axial and torsional deformability of RC members is certainly lower than that of steel members, as it is well-known.

A second issue should be considered when dealing with RC elements deformability. Clearly, for steel members, it is possible to assume a constant value of the flexural deformability coefficients up to yielding. However, the deformation of RC elements depends on their initial elastic stiffness only at low load levels. If the non-linear behaviour of concrete and steel rebars is not explicitly modelled, as in the present case, an effective deformability of members should be defined to obtain a realistic evaluation of the frame displacements given that a linear elastic behaviour is assumed for them.

In the next section, the comparison between the experimental response of test specimens and that predicted by means of Dawe and Seah's model under the hypothesis of stiff confining elements are shown, together with that calculated by accounting for the frame deformability with deformability of the RC elements equal to the initial elastic

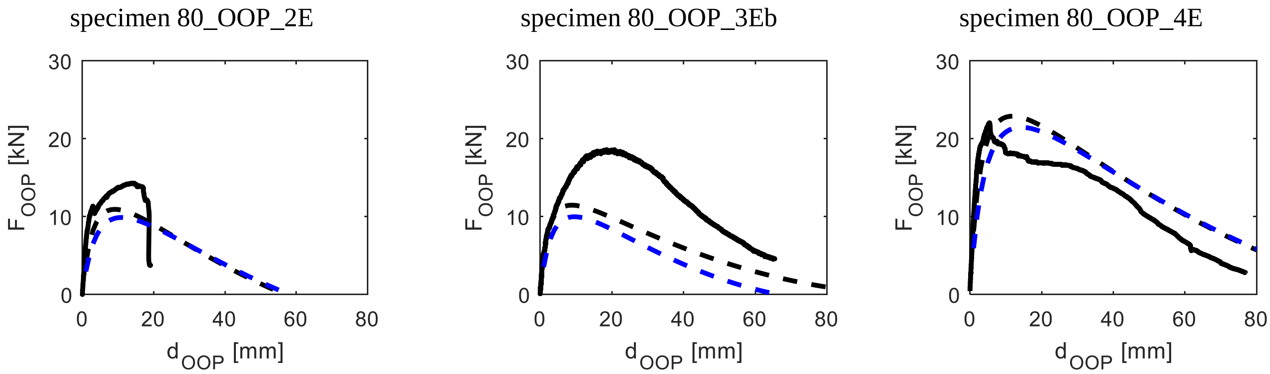

Fig. 15(a) Comparison of the experimental and theoretical response of the 80 mm-thick specimens. Experimental response: black continuous line; predicted response with stiff elements: black dashed line; predicted response with deformable elements provided of an initial elastic flexural stiffness: blue dashed line; predicted response with deformable elements provided of a reduced effective flexural stiffness: blue continuous line

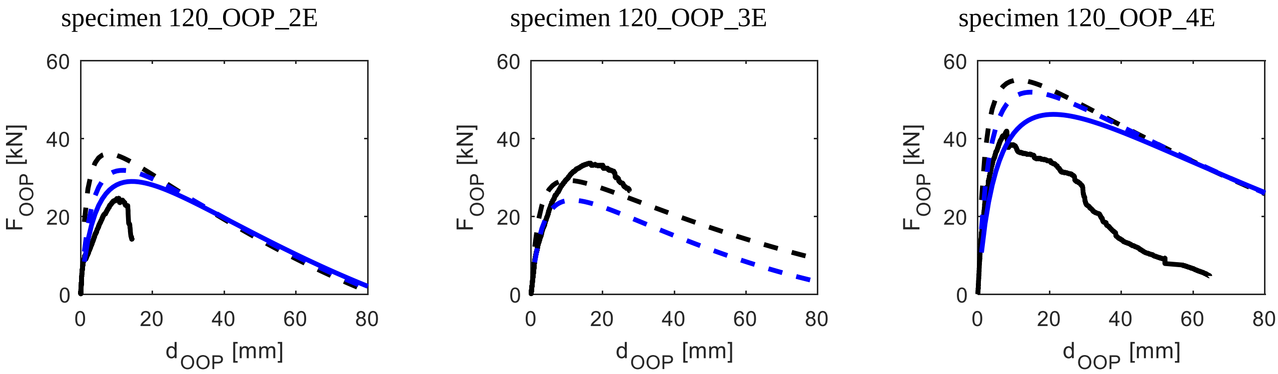

Fig. 15(b) Comparison of the experimental and theoretical response of the 120 mm-thick specimens. Experimental response: black continuous line; predicted response with stiff elements: black dashed line; predicted response with deformable elements provided of an initial elastic flexural stiffness: blue dashed line; predicted response with deformable elements provided of a reduced effective flexural stiffness: blue continuous line

one. As already stated in section 2, an LVDT was used to measure the upper beam outward deflection due to arching thrusts during tests 120_OOP_4E and 120_OOP_2E. These measures are used to calibrate the RC elements' effective deformability. The effective or "equivalent" deformability of RC elements is the one that allows predicting a maximum beam deflection equal to that observed during tests. For specimens 120_OOP_4E and 120_OOP_2E, the predictions obtained by using these values of the effective deformability are also shown.

5.3 Experimental vs predicted OOP response of specimens accounting for the frame deformability

In Fig. 15, the experimental response of specimens (black continuous line) in compared to the prediction obtained by applying Dawe and Seah's model

• with the hypothesis of stiff structural elements (black dashed line);

• with the hypothesis of deformable confining elements, by assuming a flexural stiffness of the RC elements' cross-sections equal to their gross elastic stiffness (blue dashed line).

Only for specimens 120_OOP_2E and 120_OOP_4E, a third blue continuous line is represented. Such a prediction is obtained by reducing the flexural stiffness of the RC confining elements with a certain coefficient lower than the unit, equal to 0.50 for specimen 120_OOP_2E and to 0.30 for specimen 120_OOP_4E. The reducing coefficient has been calibrated to have a predicted maximum outward displacement for the upper RC beam equal to that registered by the vertical LVDT shown in Fig. 3. For these two specimens, the experimental and predicted OOP central displacement-maximum outward beam deflection diagrams are shown and compared in Fig. 16. The experimental and predicted OOP strength values for all specimens are shown and compared in Table 3.

From Fig. 15, the following considerations can be drawn. The peak load displacement is well caught for 2E specimens, while it is underestimated for 3E specimens and slightly overestimated for 4E specimens. These trends are even more visible when introducing the confining frame deformability. For 2E specimens, it is clear that the model does not allow reproducing the load-bearing capacity drop at the attainment of peak load. This is observed also for 4E specimens. In this case, a small reduction of the OOP force was registered at peak load. This load reduction is most likely due to vertical crushing and is not reproduced by the predictive model. This is also shown in Fig. 16, in which it

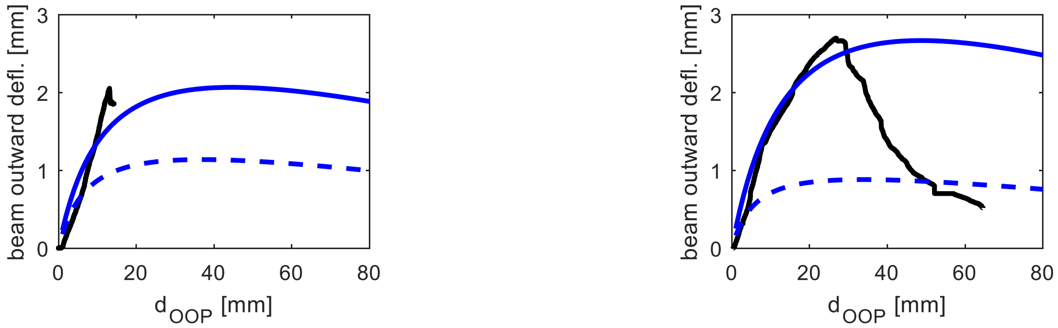

(a) (b)

Fig. 16 Comparison of the experimental and theoretical OOP central displacement-outward upper RC beam deflection diagrams obtained for specimens 120_OOP_2E (a) and 120_OOP_4E (b). The black lines refers to the experimental observation. The blue dashed lines refer to the prediction obtained by assigning an initial elastic flexural stiffness for the RC elements. The blue continuous lines refer to the prediction obtained by assigning a reduced effective flexural stiffness to the RC elements

Table 3 Comparison of the experimental and predicted values of the OOP strength of test specimens. "CoV" is for Coefficient of Variation; "stiff" is for stiff supporting elements; "deformable elastic" is for deformable supporting elements with elastic stiffness; "deformable effective" is for deformable supporting elements with effective stiffness

specimen	OOP strength (kN)						
	exp.	predicted (stiff)	exp./pred.	predicted (deformable elastic)	exp./pred.	predicted (deformable effective)	exp./pred.
80_ OOP_2E	14.6	10.9	1.34	9.9	1.47	-	-
120_OOP_2E	24.0	36.0	0.67	31.8	0.75	28.9	0.83
80_ OOP_3Eb	18.4	12.7	1.45	10.0	1.84	-	-
120_OOP_3E	33.6	30.2	1.11	24.1	1.39	-	-
80_ OOP_4E	22.0	22.3	0.99	21.4	1.03	-	-
120_OOP_4E	41.9	55.0	0.76	51.9	0.81	46.2	0.91
		mean	1.05	mean	1.22		
		median	1.05	median	1.21		
		CoV	29%	CoV	35%		

can be observed that the OOP central displacement-beam deflection relationship is well caught by the model up to the attainment of peak load: after that, the reduction of the beam deflection due to the reduction of the OOP load is not reproduced. Most likely, this occurs due to the assumption of a stress-block as masonry constitutive law, which does not allow accounting for the load-bearing capacity drop that occurs, at the attainment of masonry compressive strength, even at the material level (as shown in Di Domenico *et al.* 2018b).

In reference to the OOP strength, it is observed from Table 3 that the model is not able to reproduce the strength of 3E specimens as it systematically and significantly underestimates it (mean observed-over-predicted ratio of the subset equal to 1.28 for stiff confining frame and to 1.62 for deformable confining frame). Most likely, this occurs because the model does not account for strength sources different from arching action (e.g., masonry flexural strength). Such sources seem to be not negligible in 3E specimens, especially when considering vertical stripes.

With the exclusion of 3E specimens, focusing on 2E and 4E specimens, the prediction of the OOP strength significantly benefits from the introduction of the frame deformability with the assessment of the RC elements effective stiffness (mean observed-over-predicted ratio of the subset equal to 1.15 for 2E specimens and to 0.97 for 4E specimens). However, on the subset constituted by the 80 mm- and 120 mm-thick 2E and 4E specimens, the simple introduction of the frame deformability with initial elastic stiffness of the RC members produces satisfactory predictions, with a mean of the experimental-over-predicted ratios very close to the unit and equal to 1.02. Based on these evidences, it seems that Dawe and Seah's model can well predict the OOP strength of 2E and 4E specimens.

In addition, it seems that their complete force displacement response can be well predicted, too, provided that some modifications to the model itself are performed (i.e., the introduction of the real stress-strain relationship for masonry).

6. Conclusions

In this paper, the experimental OOP response of URM infill walls with different height-over-thickness slenderness ratio and boundary conditions at edges has been compared with the theoretical prediction obtained by applying Dawe and Seah's mechanical model, which is based on the application of the Principle of Virtual Works.

The experimental program described was dedicated to the characterization of the OOP response of URM infill walls. Six specimens equal for nominal mechanical properties and geometry, except for their thickness, were tested. Three specimens were 80 mm-thick, while the other three specimens were 120 mm-thick. For each one of these two sets, three different boundary conditions were considered. One infill was bounded on two sides, along the upper and lower edges, to the confining RC frame (2E specimens). A second infill was bounded on three sides, along the lower and lateral edges, to the confining RC frame (3E specimens). A third infill was bounded along all sides to the confining RC frame (4E specimens).

After the description of tests' results, Dawe and Seah's model is presented in detail. The mechanical principles of the model are introduced and its application is described and explained step-by-step. In addition, the introduction in the model of the confining RC frame elements' deformability is described in detail. Namely, explicit formulations, which were missing in Dawe and Seah's research, for the calculation of the RC frame deformability coefficients were presented. This detailed description of the model allows its complete and straightforward application to whichever potential user.

Finally, the model is applied and its predictions are compared with the experimental response of test specimens. It was found that the model does not predict a behaviour for 3E specimens consistent with the experimental evidences. Namely, the OOP strength of such specimens is systematically and significantly underestimated. On the contrary, especially when the RC elements' deformability is considered, the overall response of 2E and 4E specimens seems to be sufficiently well caught, as the mean of the experimental-over-predicted strength ratios is very close to the unit.

Based on this study, it seems that Dawe and Seah's model performs sufficiently well even in its original form for 2E and 4E specimens. In addition, it seems sufficiently flexible to be modified, in future works, by introducing different issues that can improve its predictive capacity for both the OOP strength and the overall OOP force-displacement relationship. Namely, the model can be modified by introducing a specific stress-strain relationship for masonry, instead of the stress-block proposed by the authors. This can allow the reproduction of certain phenomena currently not well caught, such as the load-bearing capacity drop-significant, for 2E specimens, or small, for 4E specimens-that occurs due to masonry vertical crushing at the attainment of the OOP strength. To improve the predictive capacity for 3E specimens, strength sources different from arching action (e.g., masonry flexural strength) can be introduced. In addition, a further extension of the model may be focused on the prediction of the potential switch from two-way to one-way arching during the OOP loading (a phenomenon observed, e.g., by Akhoundi *et al*. 2018).

Based on the results of this study, Dawe and Seah's model seems to deserve efforts in further investigation. The model, in fact, seems to be suitable for the proposal of a robust approach for the prediction of the OOP response and strength of URM infills.

Acknowledgments

This work was developed under the financial support of METROPOLIS (Metodologie e tecnologie integrate e sostenibili per l'adattamento e la sicurezza di sistemi urbani-PON Ricerca e Competitività 2007-2013) and ReLUIS-DPC 2014-2018 Linea Cemento Armato-WP6 Tamponature, funded by the Italian Department of Civil Protection (DPC). These supports are gratefully acknowledged.

References

Agnihotri, P., Singhal, V. and Rai, D.C. (2013), "Effect of in-plane damage on out-of-plane strength of unreinforced masonry walls", *Eng. Struct.*, **57**, 1-11.

Akhoundi, F., Vasconcelos, G. and Lourenço, P. (2018), "Experimental out-of-plane behavior of brick masonry infilled frames", *Int. J. Archit. Herit.*, In Press.

Angel, R., Abrams, D.P., Shapiro, D., Uzarski, J. and Webster, M. (1994), *Behaviour of Reinforced Concrete Frames with Masonry Infills*, University of Illinois Engineering Experiment Station, College of Engineering, University of Illinois at Urbana-Champaign.

ASCE/SEI 41-13 (2013), *Seismic Rehabilitation of Existing Buildings*, American Society of Civil Engineers, Reston, Virginia, U.S.A.

Bashandy, T., Rubiano, N.R. and Klingner, R.E. (1995), *Evaluation and Analytical Verification of Infilled Frame Test Data*, Phil M. Ferguson Structural Engineering Laboratory, University of Texas at Austin, U.S.A.

Brincker, R. (1984), *Yield-Line Theory and Material Properties of Laterally Loaded Masonry Walls*, Masonry Int.

Calvi, G.M. and Bolognini, D. (2001), "Seismic response of reinforced concrete frames infilled with weakly reinforced masonry panels", *J. Earthq. Eng.*, **5**(2), 153-185.

Dawe, J.L. and Seah, C.K. (1989), "Out-of-plane resistance of concrete masonry infilled panels", *Can. J. Earthq. Eng.*, **16**(6), 854-864.

Di Domenico, M., Ricci, P. and Verderame, G.M. (2018a), "Experimental assessment of the influence of boundary conditions on the out-of-plane response of unreinforced masonry infill walls", *J. Earthq. Eng.*, In Press.

Di Domenico, M., Ricci, P. and Verderame, G.M. (2018b), "Experimental assessment of the out-of-plane strength of URM infill walls with different slenderness and boundary conditions", *Bull. Earthq. Eng.*, Under Review.

Di Trapani, F., Cavaleri, L. and Shing, P.B. (2018), "A macro-element model for in-plane and out-of-plane responses of masonry infills in frame structures", *J. Struct. Eng.*, **144**(2), 04017198.

Edri, I.E. and Yankelevsky, D.Z. (2017), "An analytical model for the out-of-plane response of URM walls to different lateral static loads", *Eng. Struct.*, **136**, 194-209.

Eurocode 6 (2005), *Design of Masonry Structures-Part 1-1: General Rules for Reinforced and Unreinforced Masonry Structures*.

FEMA 306 (1998), *Evaluation of Earthquake Damaged Concrete and Masonry Wall Buildings*, Federal Emergency Management Agency, Washington, U.S.A.

FEMA 356 (2000), *Prestandard and Commentary for the Seismic Rehabilitation of Buildings*, Federal Emergency Management Agency, Washington, U.S.A.

Flanagan, R.D. and Bennett, R.M. (1999), "Arching of masonry infilled frames: Comparison of analytical methods", *Pract. Period. Struct. Des. Const.*, **4**(3), 105-110.

Furtado, A., Rodrigues, H., Arede, A. and Varum, H. (2016), "Simplified macro-model for infill masonry walls considering the out-of-plane behaviour", *Earthq. Eng. Struct. Dyn.*, **45**(4), 507-524.

Guidi, G., Da Porto, F., Dalla Benetta, M., Verlato, N. and Modena, C. (2013), "Comportamento sperimentale nel piano e fuori piano di tamponamenti in muratura armata e

rinforzata", *Proceedings of the 15th Conference on ANIDIS, L'Ingegneria Sismica in Italia*, Padua, Italy, July.
McDowell, E.L., McKee, K.E. and Sevin, E. (1956), "Arching action theory of masonry walls", *J. Struct. Div.*, **82**(2), 1-8.
Mosalam, K.M. and Günay, S. (2015), "Progressive collapse analysis of reinforced concrete frames with unreinforced masonry infill walls considering in-plane/out-of-plane interaction", *Earthq. Spectr.*, **31**(2), 921-943.
NTC2008 (2008), *Decreto Ministeriale 14 Gennaio 2008-Norme Tecniche Per le Costruzioni*, Supplemento Ordinario n. 30 Gazzetta Ufficiale 4 Febbraio 2008, n 29.
NZSEE 2017 (2017), *The Seismic Assessment of Existing Buildings (The Guidelines), Part C-Detailed Seismic Assessment*, New Zealand Society for Earthquake Engineering (NZSEE), Structural Engineering Society New Zealand Inc. (SESOC), New Zealand Geotechnical Society Inc., Ministry of Business, Innovation and Employment, Earthquake Commission.
Pasca, M., Liberatore, L. and Masiani, R. (2017), "Reliability of analytical models for the prediction of out-of-plane capacity of masonry infills", *Struct. Eng. Mech.*, **64**(6), 765-781.
Ricci, P., Di Domenico, M. and Verderame, G.M. (2018), "Empirical-based out-of-plane URM infill wall model accounting for the interaction with in-plane demand", *Earthq. Eng. Struct. Dyn.*, **47**(3), 802-827.

CC

Notation

The following symbols are used in this paper.

c	contact length
d_{OOP}	OOP displacement of the infill centre
E_m	masonry elastic modulus
F_{max}	OOP strength
$F(d_{OOP})$	OOP force (F) as a function of the OOP central displacement (d_{OOP})
f	outward displacement of the confining elements
f_b	brick compressive strength
f_{cm}	concrete mean compressive strength
f_j	mortar compressive strength
f_m	masonry compressive strength
f_{mv}	masonry compressive strength (vertical direction)
f_{mh}	masonry compressive strength (horizontal direction)
f_{ym}	steel rebars' mean yielding stress
g	gap between the infill and the confining structural elements
h	infill height
k_1	stress block factor
k_2	stress block factor
L	infill length in the direction of arching thrust
L_E	external virtual work
L_I	internal virtual work
M	moment due to arching thrusts
N	arching thrust
t	infill thickness
w	infill width
z	maximum OOP displacement of the generic stripe
φ	rotation of infill parts

Subscripts

h	referred to the horizontal direction
v	referred to the vertical direction